Title

Analyzing the impact of reaction models on the production of hydrocarbons from thermally upgraded oil shales

Authors

Lee, Kyung Jae
Finsterle, Stefan
Moridis, George J

Publication Date

2018-09-01

DOI

10.1016/j.petrol.2018.05.021

Peer reviewed

Analyzing the impact of reaction models on the production of hydrocarbons from thermally upgraded oil shales

Kyung Jae Lee[ab] Stefan Finsterle[bc] George J. Moridis[bd]

Abstract

Reaction parameters significantly affect oil production from shales by means of heating and in-situ upgrading. In this study, we perform numerical simulations of two chemical reaction models, which are mainly used in the research of kerogen pyrolysis and subsequent hydrocarbon decomposition in organic-rich porous media. They are the Braun and Burnham model and Wellington model. In these forward numerical simulations, we present the influence of the two reaction models on hydrocarbon production. The Braun and Burnham reaction model shows more vigorous kerogen and subsequent decomposition reactions and more hydrocarbon production than the Wellington model. A local sensitivity analysisidentifies the reaction parameters with the highest influence on productivity, and the most sensitive outputs. A data-worth analysis identifies the most valuable observation data to be measured for the best prediction of total hydrocarbon production. We find that the most valuable observation data is the cumulative production of heavy oil in the Braun and Burnham model and of light oil in the Wellington model, respectively. Once we determine the maximum allowable prediction uncertainty and the expected measurement uncertainty, the observation data to be measured for the minimization of prediction uncertainty can be obtained.

Keywords: In-situ upgrading, Oil shale, Numerical simulation, Sensitivity analysis, Uncertainty prediction, Data-worth analysis

1. Introduction

Oil shale is a valuable source of fossil fuel with significant known resources of 8 trillion barrels in 27 countries worldwide (Ogunsola et al., 2010). Six trillion barrels of resources are concentrated in the US, and two trillion barrels among them are estimated to have a commercial value. However, hydrocarbon production of commercial scale from oil shale has not been accomplished because of the technical and economic challenges associated with the thermal upgrading process. The challenges are caused by diverse factors, including uncertainty of the reservoir properties and of the kinetic parameters of the reactions occurring during the thermal upgrading of oil shale.

Sensitivity analyses of system responses to the reservoir properties and the reaction parameters have been conducted in several previous studies. The sensitivity of hydrocarbon production to the initial fluid porosity, the initial content of organic matter, the spacing of the fracture network, and the initial saturation of the various fluid phases was quantified (Lee et al., 2016, 2017). In the study of parameter space reduction, a statistical methodology

involving designed factorial experiments was developed to analyze the effects of the molecular weight of kerogen and of the activation energies of reactions, and to estimate the uncertainty of the hydrocarbon recovery (Bauman and Deo, 2010). In that study, the dynamic system changes were ignored, including the permeability evolution, the rock expansion, and the pore-plugging by solid cokes generated from the reactions of thermal upgrading. In the study of inverse modeling of reactivity using temperature transient data, the effects of reaction parameters and oil shale grade on the electrical heater temperature were quantified (Lee et al., 2018).

Uncertainty of reservoir properties is a persistent problem not only in oil shale reservoirs but also in many conventional and unconventional hydrocarbon reservoirs. On the other hand, uncertainty in the reaction models and in the parameters of the decomposition reactions of kerogen, hydrocarbons, and cokes is only relevant in the application of in-situ upgrading in oil shale reservoirs. Little in-depth research has been conducted regarding the uncertainty of chemical reaction models and reaction parameters.

In this study, we evaluate the effects of chemical reaction models and of the values of the reaction parameters (involved in the thermal upgrading processes of kerogen, hydrocarbons, and cokes) on hydrocarbon production. The main focus of our effort is to analyze the effects of uncertainty in the reaction models on the prediction of hydrocarbon production. There is a number of chemical reaction models of kerogen pyrolysis and subsequent hydrocarbon decomposition (Braun and Burnham, 1990, 1992; Burnham and Braun, 2017; Campbell et al., 1978; Fucinos et al., 2017; Pepper and Corvi, 1995; Pepper and Dodd, 1995; Reynolds et al., 1991; Wellington et al., 2005).

We investigate the following two reaction models: The Braun and Burnham model (Braun and Burnham, 1992) and the Wellington model (Wellington et al., 2005), which have been frequently used in relevant studies. These two reaction models were obtained from the samples of different reservoirs, and have different reaction parameters.

This paper describes the simulation process and specifications, and the related solutions obtained from forward modeling, sensitivity and data-worth analyses. In forward modeling, we simulate the in-situ upgrading process of oil shale by applying the Shell In-situ Conversion Process (ICP), which heats the oil shale formation using multiple vertical electric heaters installed in a hexagonal pattern. We consider the effects of reaction parameters on system responses, which will be different in the two reaction models mentioned above. We estimate and compare the hydrocarbon production, reactivity, pressure, temperature, saturations of phases, effective porosity, and kerogen volume fraction, which are obtained with the two reaction models.

A local sensitivity analysis is performed to assess the relative influence of various reaction parameters on the system response. Using these parameters and the corresponding system responses, a data-worth analysis is performed to identify the most valuable data to be measured during in-situ upgrading and production, and to reduce the prediction uncertainty of the total hydrocarbon production.

The purpose of this study is to evaluate 1) the difference of system responses calculated by the Braun and Burnham model and the Wellington model, 2) the most influential reaction parameters that significantly affect the system responses, 3) valuable data that should be measured to reduce the prediction uncertainty of hydrocarbon production, and 4) the uncertainly of the predicted hydrocarbon production.

2. Numerical simulation code for in-situ upgrading of oil shales

We use our in-house numerical simulation code (Lee et al., 2016) developed based on a variant of TOUGH+ (Moridis et al., 2006), which is a member of the TOUGH2 family of codes developed by staff at the Lawrence Berkeley National Laboratory (Pruess et al., 1999). It describes relevant physical, thermodynamic, and chemical phenomena that occur during the in-situ upgrading processes in oil shale reservoirs. Confidence in the code was gained by comparing simulation results with field production data obtained in the Green River Formation (Fowler and Vinegar, 2009; Lee et al., 2016; Vinegar, 2006).

2.1. Governing equations

The in-situ upgrading of oil shale involves physical, thermodynamic, and chemical phenomena under dynamically changing conditions. These phenomena are mathematically described by the equations of mass and energy balance, and by relevant chemical reactions.

The mass balance equation accounts for mass accumulation of various components, source and sink effects, component mass changes caused by chemical reactions, and mass flux terms across the boundaries of any control volume as follows.

$$(1)\partial\partial t(\sum\beta\equiv A,O,G,S\varnothing S\beta\rho\beta X\beta\kappa)=\sum\beta\equiv A,O,GqX\beta\kappa+\sum kMk\kappa-\nabla\cdot(\sum\beta\equiv A,O,Gkkr\beta\rho\beta\mu\beta(\nabla p\beta-\rho\beta g)X\beta\kappa)$$

On the left-hand side of Eq. (1), φ is the media porosity retaining four phases —aqueous (*A*), liquid organic (*O*), gaseous (*G*), and solid (*S*); Sβ is the saturation of phase β; ρβ [$kg\cdot m^{-3}$] is the density of phase β; and Xβκ is the mass fraction of component κ in phase β. Note that the solid phase is included in the media porosity to calculate its dynamically changing amount caused by the decomposition reactions. On the right-hand side of Eq. (1), qβ[$kg\cdot m^{-3}\cdot s^{-1}$] is the sink term of phase β; Mkκ [$kg\cdot m^{-3}\cdot s^{-1}$] is the mass change by *k*-th reaction of component κ ; k [m^2] is the absolute permeability; krβ is the relative permeability of phase β; μβ [Pa·s] is the viscosity of phase

β; pβ [Pa] is the pressure of phase β; and g[m·s^{-2}] is the gravity vector, respectively. In this mass balance equation, diffusive flux and sorption effect were not included for the efficient computation, regarding their insignificant impact in our problem.

The reaction rates of the thermal decomposition reactions of kerogen, hydrocarbons and cokes are computed by using first-order reactions based on Arrhenius law (Braun and Burnham, 1992; Fan et al., 2010; Maes et al., 2017; White et al., 2010; Youtsos et al., 2013):

(2)rk=KkCκ

where, rk [kg·m^{-3}·s^{-1}] is the reaction rate of the *k*–th reaction; Kk [s^{-1}] is the reaction rate constant of the *k*–th reaction; and Cκ [kg·m^{-3}] is the concentration of component κ . Here, Kk and Cκ are computed as follows:

(3)Kk=Akexp(−Ek/(RT))

(4)Cκ=φ∑β≡A,O,G,SSβρβXβκ

where, Ak [s^{-1}] is the frequency factor of *k*–th reaction; Ek [kJ·mole^{-1}] is the activation energy of *k*–th reaction; R [kJ·mole^{-1}·K^{-1}] is the gas constant; and T [K] is the system temperature, respectively. Considering Eq. (2), the mass change caused by the chemical reactions in Eq. (1) is described as follows.

(5)∑kMkκ=∑krkskκ

where, skκ is the stoichiometric coefficient of component κ in the *k*–th reaction as a mass fraction.

The energy balance equation accounts for heat accumulation, the thermal effects of sources and sinks, the enthalpy of the various chemical reactions, and the heat flux terms across the boundaries of any control volume, and is described as follows:

(6)∂∂t((1−∅)ρRCp,RT+∅∑β≡A,O,G,SρβUβSβ)=∇(K∇T)−∇·(∑β≡A,O,GρβhβFβ) +∑β≡A,O,Gqβhβ+∑kΔhkrk

where, ρR [kg·m^{-3}] is the dry rock density; Cp,R [J·kg^{-1}·K^{-1}] is the specific heat capacity of dry rock; Uβ [J·kg^{-1}] is the internal energy of phase β; K [W·m^{-1}·K^{-1}] is the composite thermal conductivity of formation; hβ [J·kg^{-1}] is the specific enthalpy of phase β; Fβ [m^{3}·s^{-1}] is the flux of phase β; and Δhk [J·kg^{-1}] is the reaction enthalpy of the *k*-th reaction. Here, Fβ is computed by the Darcy equation as shown in the last term on the right-hand side of Eq. (1).

2.2. Chemical reaction models

In this study, two different chemical reaction models are covered. The first is the most widely used model of Braun and Burnham model (hereafter referred to as the BB-model) (Braun and Burnham, 1992). It includes seven chemical reactions occurring during the in-situ upgrading of oil shale. The seven reactions are the decompositions of kerogen, heavy oil, light oil,

hydrocarbon gas, coke 1, coke 2, and coke 3. Table 1 shows the reaction details.

Table 1. Braun and Burnham (BB) reaction model (Braun and Burnham, 1992). Note that the stoichiometric coefficients are mass fraction-based.

Reactions	Frequency factor [s^{-1}]	Activation energy [$kJ \cdot mole^{-1}$]	Reaction enthalpy [$kJ \cdot mole^{-1}$]	Magnitude of reaction rate constant[a] [s^{-1}]
Kerogen → 0.279 Heavy oil + 0.143 Light oil + 0.018 Hydrocarbon gas + 0.005 Methane + 0.555 Coke 1	3.0×10^{13}	213.384	−335	10^{-8}-10^{-5}
Heavy oil → 0.373 Light oil + 0.156 Hydrocarbon gas + 0.03 Methane + 0.441 Coke 2	1.0×10^{13}	225.936	−46.5	10^{-10}-10^{-6}
Light oil → 0.595 Hydrocarbon gas + 0.115 Methane + 0.290 Coke 3	5.0×10^{11}	225.936	−46.5	10^{-11}-10^{-8}
Hydrocarbon gas → 0.682 Methane + 0.318 Coke 4	1.2×10^{12}	238.488	−46.5	10^{-12}-10^{-8}
Coke 1 → 0.031 Hydrocarbon gas + 0.033 Methane + 0.936 Coke 2	1.0×10^{13}	225.936	−46.5	10^{-10}-10^{-6}
Coke 2 → 0.003 Hydrocarbon gas + 0.033 Methane + 0.964 Coke 3	5.0×10^{11}	225.936	−46.5	10^{-11}-10^{-8}
Coke 3 → 0.018 Methane + 0.982 Coke 4	1.2×10^{12}	238.488	−46.5	10^{-12}-10^{-8}

a

Magnitudes of reaction rate constants were computed under temperature between 250 and 350 °C.

The second model is the Wellington model (Wellington et al., 2005) (hereafter referred to as the W-model), which includes different decomposition reactions than those of the BB-model. The details of six reactions in the W-model are provided in Table 2. Here, several adjustments are made for a more realistic description of chemical kinetics (Lee et al., 2016). Please note that every reaction enthalpy was reported as zero in the W-model; thus it is not accounted in our simulations. The frequency factor of kerogen decomposition has been obtained from the adjusted W-model (Fan et al., 2010), which is close to a linear sum of frequency factor values under high and low pressure. The frequency factors of heavy and light oil decompositions have been obtained from a table originally proposed by Wellington (Wellington et al., 2005) in order to produce similar reaction rates to the generally known values. The stoichiometric coefficients of the gaseous and liquid organic phases of heavy oil decomposition have been swapped, because it is scientifically more convincing that liquid organic phase would

produce more oil than gas, and that a gaseous phase would produce more gas than oil.

Table 2. Adjusted Wellington (W) reaction model (Fan et al., 2010; Lee et al., 2016; Wellington et al., 2005). Note that the stoichiometric coefficients of reactions have been adjusted to mass fractions, which were originally described as mole-based.

Reactions	Frequency factor [s^{-1}]	Activation energy [$kJ \cdot mole^{-1}$]	Reaction enthalpy [$kJ \cdot mole^{-1}$]	Magnitude of reaction rate constant[a] [s^{-1}]
Kerogen → 0.032H_2O + 0.0014H_2 + 0.016 CO_2 + 0.20 Heavy oil + 0.18 Light oil + 0.079 Hydrocarbon Gas + 0.49 Prechar	4.33×10^{7}	161.600	–	10^{-9}-10^{-6}
Heavy oil (G) → 0.10 Light oil + 0.20 Hydrocarbon Gas + 0.70 Prechar	9.20×10^{11}	206.034	–	10^{-9}-10^{-6}
Heavy oil (O) → 0.898 Light oil + 0.004 Hydrocarbon Gas + 0.098 Prechar	9.20×10^{11}	206.034	–	10^{-9}-10^{-6}
Light oil (G) → Hydrocarbon Gas	6.77×10^{11}	219.328	–	10^{-11}-10^{-7}
Light oil (O) → 0.10 Hydrocarbon Gas + 0.90 Prechar	6.77×10^{11}	219.328	–	10^{-11}-10^{-7}
Hydrocarbon gas → 0.21H_2 + 0.79 Char	8.87×10^{15}	311.432	–	10^{-16}-10^{-11}

a

Magnitudes of reaction rate constants were computed under temperature between 250 and 350 °C.

The reaction rate constants of the decomposition reactions in each reaction model are shown in Fig. 1, and are also summarized in Table 1. In the BB-model, the reaction rate constants of the kerogen, heavy oil, and coke 1 decompositions are relatively higher than those for the other reactions. In the W-model, the reaction rate constants of decompositions of kerogen and heavy oil are relatively higher than those in the other reactions.

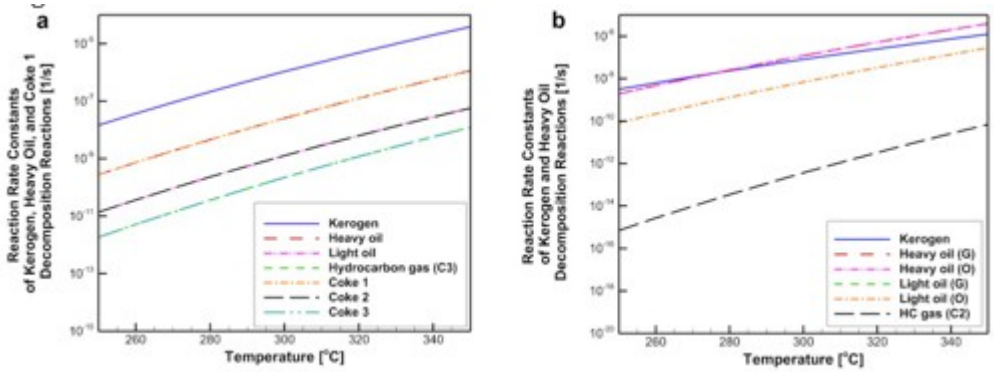

Fig. 1. Reaction rate constants of the two reaction models. (a) BB-model, (b) W-model.

As presented in the chemical reaction models, our system involves multiple phases, i.e. 1) aqueous, 2) liquid organic, 3) gaseous, and 4) solid phases. The aqueous phase is mainly composed of liquid water with dissolved oil and gas components. The liquid organic phase is mainly composed of liquid oil with dissolved water and gas components. The gaseous phase is composed of free gas components and vapors of water and oil (organic components). The solid phase is initially composed of immature hydrocarbon, kerogen. Solid products of cokes and chars are generated from the reactions.

The BB-model includes ten components: 1) water, 2) heavy oil (C24), 3) light oil (C9), 4) methane gas (C1), 5) mixed hydrocarbon gas (C3), 6) kerogen, 7) coke 1, 8) coke 2, 9) coke 3, and 10) coke 4. Water does not exist in the chemical reactions of the BB-model, but we include it because the aqueous phase occupies a portion of porosity. In the W-model, nine components are present: 1) water, 2) heavy oil (C22), 3) light oil (C11), 4) mixed hydrocarbon gas (C2), 5) hydrogen, 6) carbon dioxide, 7) kerogen, 8) prechar, and 9) char.

2.3. Dynamic system changes during in-situ upgrading

During in-situ upgrading, phase properties are dynamically changing by the alteration of system conditions—the increase of pressure and temperature caused by heating, the change of the component concentrations caused by the chemical reactions, phase transitions, fluid transport, evolution of porosity and permeability, heat transport by conduction and convection, and pressure decrease caused by fluid production in the vicinity of wells.

The dynamic thermophysical and transport properties of phases are computed considering the species and fractions of the individual components present in the phases. The properties of each individual component are computed as a function of pressure and temperature, whereby appropriate mixing rules are applied. The detailed description of the computation of thermophysical and transport properties, such as density, viscosity, specific enthalpy, and thermal conductivity, can be found in the paper on the simulator development (Lee et al., 2016).

Given that most oil shale reservoirs have high contents of calcareous minerals (and are thus highly fractured), our simulation model invoked its capability to describe naturally fractured reservoirs by the Multiple Interacting Continua (MINC) (Pruess, 1985) concept. MINC describes fractured media by two or more subdomains of connected fracture-and-matrix continua. The matrix domain contains solid kerogen in its pores and expels converted fluid to the fracture domain as kerogen decomposition and subsequent decompositions occur. The connected fracture domain provides the pathways for fluid transport and convective heat flow.

The initial matrix porosity of raw oil shale is very small, and it increases as pores expand following the temperature increase and pressurization by heating. As temperature gets sufficiently high for kerogen decomposition,

matrix porosity rapidly increases by the replacement of solid kerogen by fluid and solid products. The numerical simulator fully describes the evolution of matrix porosity and permeability, as well as the heat flow by convection between matrix and fracture domains, which becomes progressively dominant as the porosity and permeability of the matrix increase. The simulator also accounts for the effect on the matrix porosity and permeability caused by the generation of solid products of the upgrading process (cokes, char, and prechar) and by the kerogen decomposition. The dependence of the permeability of the matrix domain on the porosity is computed using the modified Kozeny-Carman equation (Krauss and Mays, 2014).

The simulator contains multiple options for relative permeability and capillary pressuremodels (Lee et al., 2016). In this study, we used (a) the van Genuchten model (two phases) and the Parker et al. model (three phases) to describe the relative permeability and the capillary pressure in the rock matrix, and (b) the Stone model for the relative permeability in the fracture continuum (Parker et al., 1987; Stone, 1970; Van Genuchten, 1980). No capillary pressure effect was included in the fractures.

The reactivity of each reactant in the decomposition reactions also changes dynamically. As can be seen in Eqs. (2), (3), (4), the reaction rate is a function of the reaction parameters, the temperature, and the reactant concentration. Reactants of decomposition reactions other than kerogen decomposition in Table 1, Table 2 are the products of other reactions; the reactivities of each reactant are affected by each other.

3. Problem setup

We use a 2D conceptual model mimicking the installation of heaters and producers of Mahogany Demonstration Project-South (MDP-S), which had been implemented by Shell in the Green River Formation from 2003 to 2005 (Fowler and Vinegar, 2009). We use a 2D model because of its computational efficiency, in light of the recent study (using a scaling analysis) that revealed that gravitational effects were not important in an in-situ upgrading configuration with densely installed electric heaters and producers (Maes et al., 2017). The reservoir configuration and grid system of our model are shown in Fig. 2. The conceptual model of Fig. 2 (a) includes 16 electric heater wells arranged in a hexagonal pattern, with two producers drilled at the center of the heater pattern. Our reservoir model for the numerical simulations involves a quarter of the conceptual model as can be seen in Fig. 2(b). The model thickness is 34.44 m, which represents the length of the MDP-S heaters. The initial conditions are listed in Table 3. The fracture network was represented using the MINC approach with a fracture spacing of 3 m that represents both the natural and thermally induced fractures. The reservoir properties and input parameters were homogeneous in the initial condition, but the properties including matrix porosity, permeability, kerogen

volume fraction, and thermophysical properties of fluids and rock became heterogeneous as heating and kerogen decomposition proceeded.

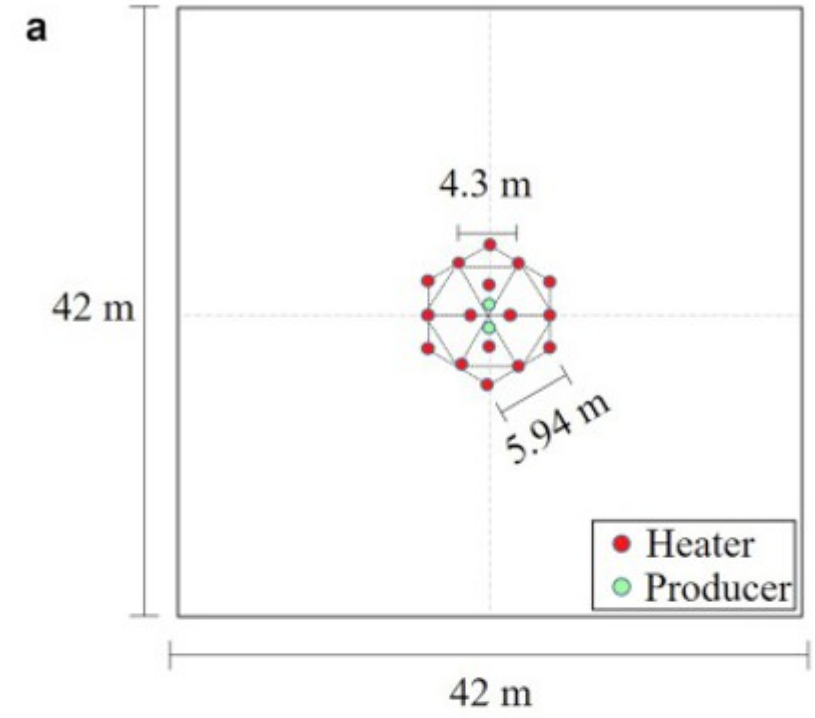

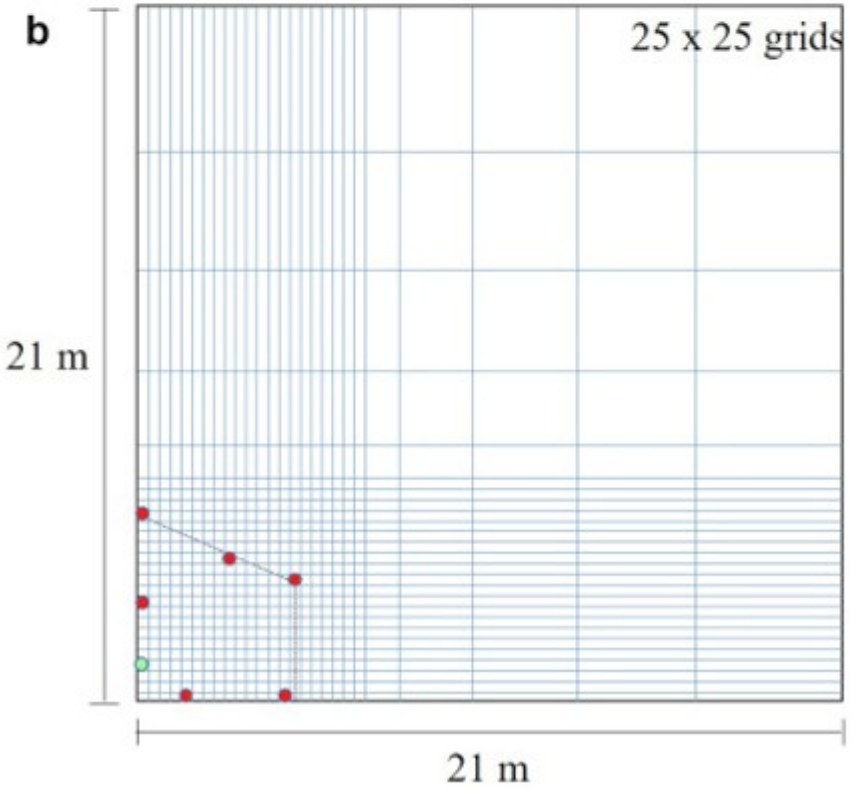

Fig. 2. (a) Conceptual model setup, (b) reservoir model for the numerical simulations (Lee et al., 2016).

Table 3. Initial conditions of reservoir properties and input parameters.

Initial condition	Value
Pressure [MPa]	25
Temperature [°C]	35
Effective porosity of matrix [−]	0.04
Absolute permeability of matrix [m^2]	1.23×10^{-16}
Volume fraction of kerogen in bulk oil shale [%]	25
Oil shale grade [gpt]	20
S_A in void pores and fractures [−]	1.0
Spacing of fracture network in MINC [m]	3
Fracture domain volume fraction [−]	0.01
Fracture domain permeability [m^2]	1.23×10^{-13}

We simulated the heating and production for 400 days. The heater temperature was maintained at a constant value of 335 °C, which is in the range of heater temperatures that were used when obtaining maximum production with densely installed electric heaters (Maes et al., 2017). Fluids were produced at the two producers during the heating process by using a linearly decreasing bottomhole pressure, reaching a final pressure reduction of 10 MPa (over the initial one) at the end of the heating and production phase.

4. Methodology of sensitivity and data-worth analyses

We analyzed the relation between the unknown or uncertain input parameters and the corresponding output variables using the simulation-optimization framework of iTOUGH2 (Finsterle, 1999; Finsterle and Zhang, 2011), in combination with the PEST protocol, which was used to link our forward numerical simulator to the iTOUGH2 analysis toolset. We performed a local sensitivity analysis by perturbing the decomposition reaction parameters of the two reaction models. This analysis may help identify the most influential reaction parameters and the most sensitive system responses. Next, we performed a data-worth analysis to determine the relative contribution that measurable system responses made to the reduction of the uncertainty in model predictions of total hydrocarbon production.

4.1. Local sensitivity analysis

The local sensitivity analysis computes the sensitivity coefficients, defined as partial derivatives of output responses to input parameters.

(7)Sij=∂zi∂pj

Here, Sij is the sensitivity coefficient of the *i*-th output response, zi, to the *j*-th parameter, pj. Next, the sensitivity coefficients are scaled by the expected variability and uncertainty of the input and output, respectively, to make them dimensionless and comparable to each other.

(8)S¯ij=Sijσpjσzi

Here, σpj is the parameter scaling factor; and σzi is the output scaling factor. A detailed discussion and interpretation of these factors can be found in (Finsterle, 2015).

The uncertain input parameters are those of the decomposition reaction models; and the output response of interest is the hydrocarbon production.

4.2. Data-worth analysis

The data-worth analysis investigates the relative worth of measurable data to reduce the uncertainty in the prediction of interest. Evaluation of each data worth is based on the local sensitivity analysis and a notional inversion. The procedure is as follows (Finsterle, 2015; Wainwright and Finsterle, 2016).

1) Select observable variables, which will be computed by forward simulations. The observable variables are categorized into actual and potential observations, and the target prediction of interest.

2) Select parameters potentially affecting the prediction of interest.

3) Calculate sensitivity coefficients, Sij , for all observations and predictions with respect to all selected parameters.

4) Compute the covariance matrix of the estimated parameters, Cpp:

(9)Cpp=s02(JTCzz−1J)−1

where, s02 is the estimated error variance, which is set to 1 in our case because of the absence of actually measured data; J is the Jacobian matrix containing the sensitivity coefficients, Sij .

5) Propagate the uncertainty of the estimated parameters, Cpp, to the prediction uncertainty, Czˆzˆ.

(10)Czˆzˆ=JˆCppJˆT

where, Jˆ is the Jacobian matrix only containing the sensitivity coefficients of predictions.

6) Remove one of the actual observations (*k*), and estimate the covariance matrix, Cpp,−k.

7) Estimate the covariance matrix of the model predictions, Czˆzˆ,−k, by inserting Cpp,−kinto Eq. (10).

8) Scale the prediction covariance matrices by acceptable prediction uncertainty, to get $C^{-}z^{\wedge}z^{\wedge}$ and $C^{-}z^{\wedge}z^{\wedge},-k$.

9) Evaluate data worth of each actual observation by a relative increase of prediction uncertainty by the removal of observation (k).

$$(11)\omega-k=1-\mathrm{tr}(Cz^{\wedge}z^{\wedge})\mathrm{tr}(Cz^{\wedge}z^{\wedge},-k)$$

where, $\omega-k$ is the relative data worth of observation (k).

5. Results of forward simulations

Now we discuss the numerical simulation results of in-situ upgrading in the cases of the BB- and the W-model. All reservoir properties, initial conditions, and heating and production processes were identical in the two cases, except for the reaction model, the reaction parameters, and the involved components.

Fig. 3 presents the distribution profiles of kerogen volume fraction in the solid phase during the in-situ upgrading process. By comparing them, we find that kerogen decomposed more actively when using the BB-model due to the 5 to 30 times larger reaction rate constant of kerogen decomposition in the BB-model than in the W-model (see Fig. 1).

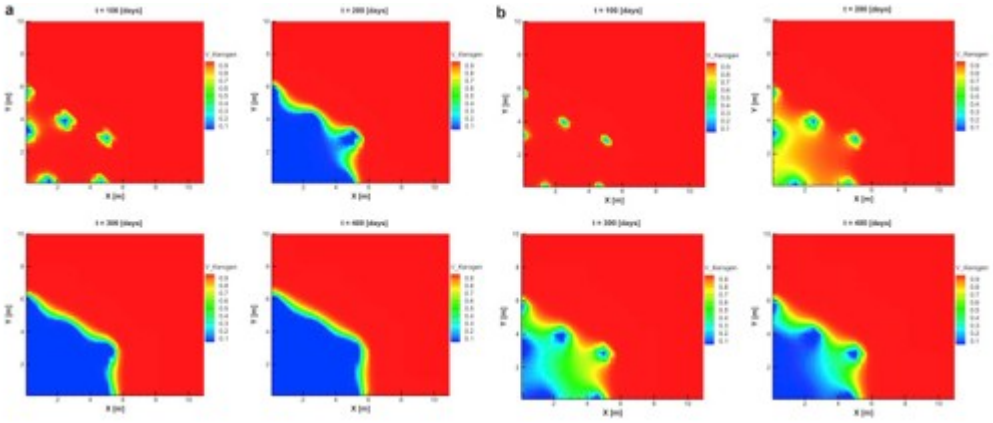

Fig. 3. Distributions of kerogen volume fraction in solid phase. (a) BB-model, (b) W-model.

Fig. 4 presents the cumulative productions of fluid components and phases in the case of BB-model. Fig. 4 (a) indicates that the cumulative water production was the largest of all components. This was caused by the fact that the void spaces of pores and fractures were initially filled with the aqueous phase, dominated by liquid water. The cumulative productions of heavy oil, light oil, and hydrocarbon gases of C3 and C1 followed the water production. Fig. 4 (b) shows the highest cumulative production of liquid organic phase among the phases followed by gaseous phase and aqueous phase, by the active generation of liquid organic phase from kerogen decomposition.

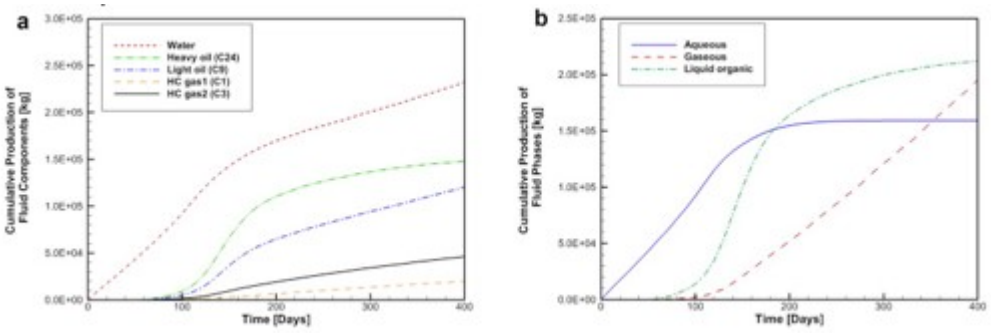

Fig. 4. Cumulative productions in the case of BB reaction model. (a) fluid components, (b) fluid phases.

Fig. 5 shows the system response during the in-situ upgrading process using the BB-model. Fig. 5 (a), (b), and (d) present the system variables measured at the monitoring point located at $x = 2.52\,\text{m}$ and $y = 2.88\,\text{m}$, which is the center of the heating area in the simulation model.

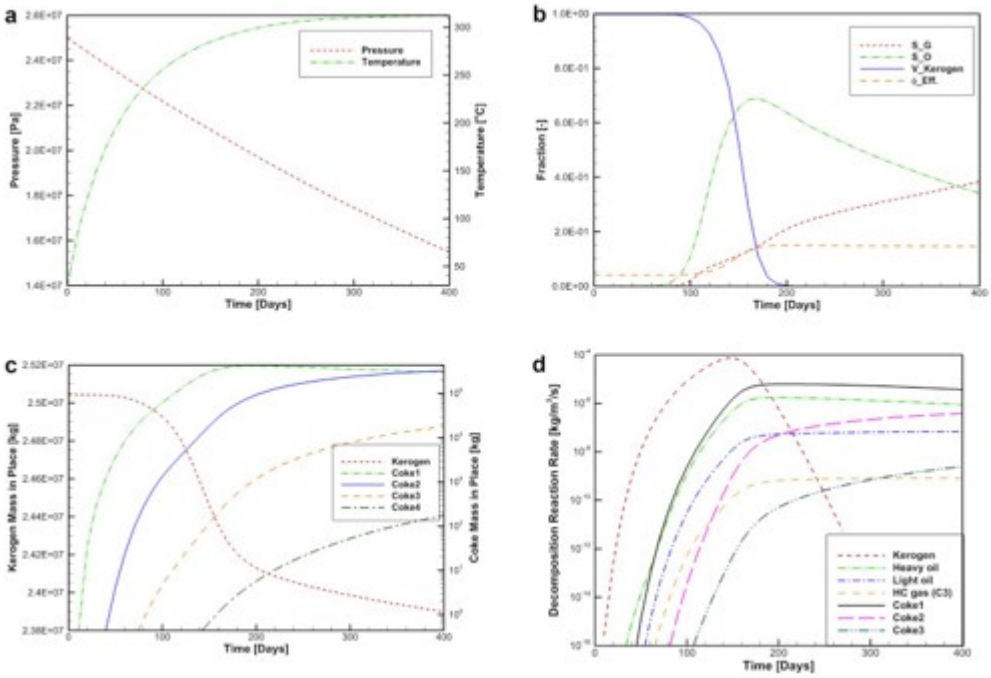

Fig. 5. System responses in the case of BB-model. (a) pressure and temperature at the monitoring point, (b) phases saturations, kerogen volume fraction in solid phase, and effective porosity at the monitoring point, (c) masses in place of solid components in the system, (d) decomposition reaction rates at the monitoring point.

Note that the phase saturations in (b) are the scaled values by the total saturation of fluid phases.

Fig. 5 (a) shows that the pressure at the monitoring point gradually decreased, being affected by the flowing bottomhole pressure of the production well, which was decreased linearly during the heating and production processes. The temperature at this monitoring point gradually increased by heating and approached a plateau at around $t = 320$ days.

Fig. 5 (b) shows the evolutions of the effective porosity, the scaled saturations of phases, and the kerogen volume fraction. The saturations of the liquid organic and gaseous phases were scaled by the total saturation of fluid phases, and were computed as follows:

$$(12) SO* = \frac{SO}{SA + SO + SG}$$

$$(13) SG* = \frac{SG}{SA + SO + SG}$$

where, $SO*$ and $SG*$ are the scaled saturation of liquid organic phase and gaseous phase, respectively.

Kerogen at the monitoring point actively decomposed starting at $t = 100$ days, and its volume fraction approached zero at $t = 280$ days. The scaled saturation of the liquid organic phase peaked at $t = 170$ days, and decreased afterwards in response to the kerogen decomposition and production of oil. The scaled saturation of the gaseous phase increased continuously because of the decomposition of oil components, the vaporization of water and of the oil components, and the dominant production of liquid organic phase, as shown in Fig. 4 (b). The effective porosity of the matrix at the monitoring point increased after $t = 100$ days because of the active decomposition of kerogen, and approached the plateau of 0.145 at $t = 180$ days.

Fig. 5 (c) shows the mass of solid components in the system. The total mass of decomposed kerogen was 1.15×10^6 kg. Coke 1, 2, 3, and 4 appeared in the system at $t = 10$, 40, 68, and 142 days, and the generated mass of each one of them was 3.00×10^5, 3.39×10^5, 1.89×10^4, and 187 kg, respectively, at the end of the process. Note that the mass in place of coke 1 peaked at $t = 200$ days, after which it decreased slowly because of its decomposition reaction.

Fig. 5 (d) shows the evolution of the reaction rates at the monitoring point. As can be seen from Eq. (2), the reaction rate is a function of the system temperature and of the concentration of the reactants. The reaction rate of kerogen approached its maximum value of 7.65×10^{-5} kg m^{-3} s^{-1} at $t = 150$ days, and then declined, approaching zero at about $t = 270$ days.

The cumulative productions in the case of the W- model are shown in Fig. 6. Water was the main component produced, followed by light oil, hydrocarbon gas (C2), heavy oil, CO_2, and H_2. As can be seen in Fig. 6 (b), the gaseous and liquid organic phases showed the highest and the lowest cumulative productions, respectively, among the various phases. Compared to the BB-model, less liquid organic phase was produced because a smaller amount of kerogen decomposed in the W-model.

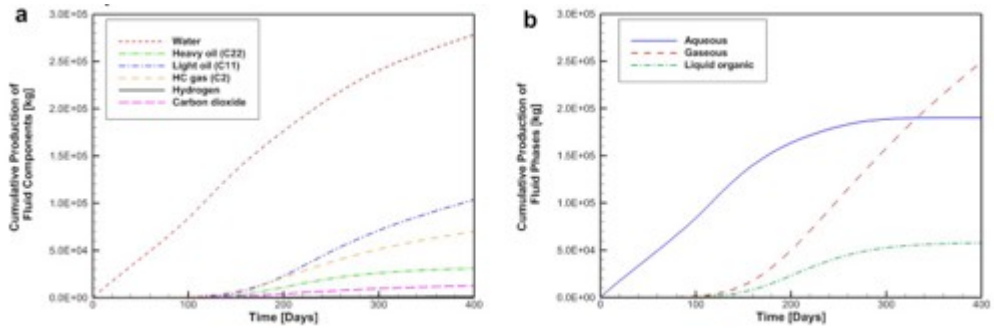

Fig. 6. Cumulative productions in the case of W-model. (a) fluid components, (b) fluid phases.

The system responses at the monitoring point of $x = 2.52\,\text{m}$ and $y = 2.88\,\text{m}$ are provided in Fig. 7. The temperature increased slower than in the BB-model because of the smaller increase of porosity and permeability caused by the lower kerogen decomposition, and, consequently, the lower convective heat flow in the W-model (Fig. 7 (a)). As can be seen in Fig. 7 (b), kerogen persisted at the monitoring point after heating and production. The scaled saturation of liquid organic phase approached 0.52, which was higher than that of 0.34 in the BB-model. The effective porosity continuously increased, starting at $t = 140$ days and approaching 0.148 at the end of the process.

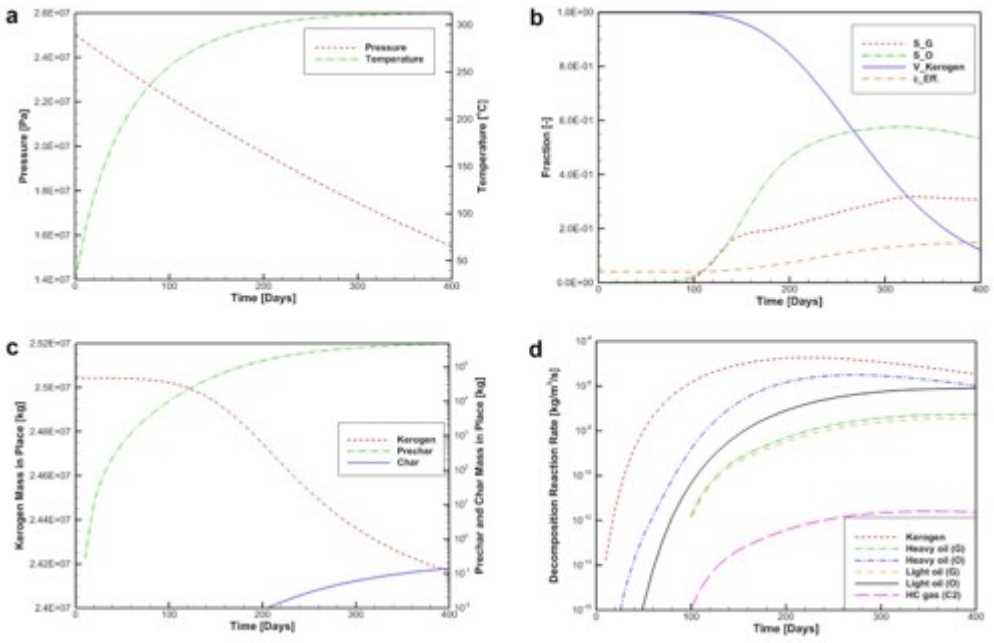

Fig. 7. System responses in the case of W-model. (a) pressure and temperature at the monitoring point, (b) phases saturations, kerogen volume fraction in solid phase, and effective porosity at the monitoring point, (c) masses in place of solid components in the system, (d) decomposition reaction rates at the monitoring point.

Note that the phase saturations in (b) are the scaled values by the total saturation of fluid phases.

Fig. 7 (c) indicates that the total mass of decomposed kerogen in the system was 8.90×10^5 kg. The mass of the generated prechar was 4.76×10^5 kg; and the mass of the generated char was less than 0.2 kg. Fig. 7 (d) shows that the reaction rate of the kerogen decomposition remained high until the end of the process. The reaction rates of the oil components were higher in the liquid organic phase than in the gaseous phase because of their higher concentration in the liquid organic phase. The reaction rate of the C2 gas showed much lower values than other reactions because of its lower reaction rate constant.

Fig. 8 shows the cumulative productions of fluid phases in the BB-model and the W-model together. More productions of aqueous and gaseous phases were observed in the W-model, while more production of liquid organic phase was observed in the BB-model.

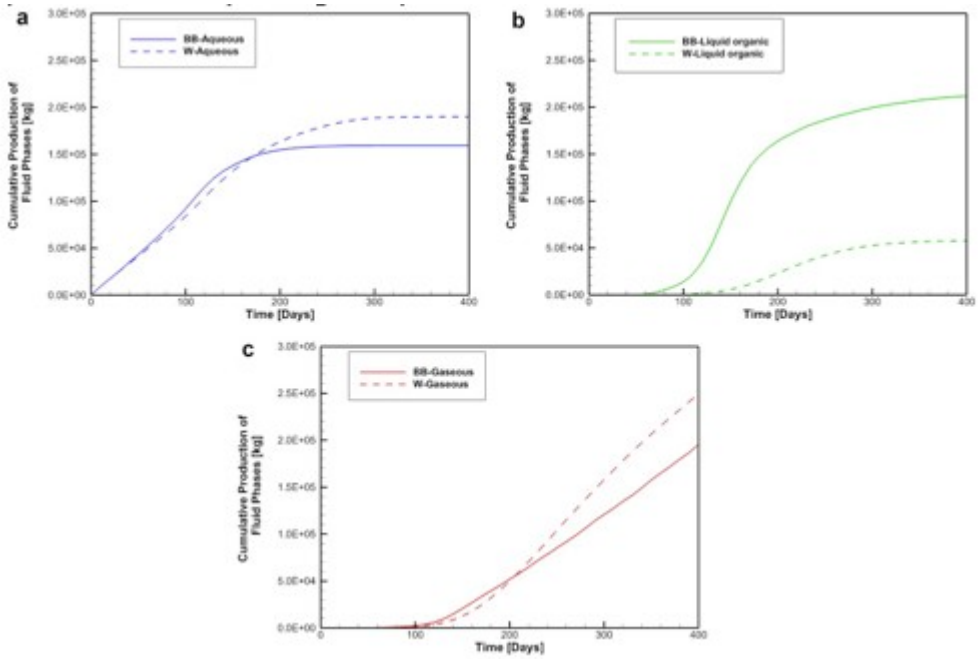

Fig. 8. Cumulative productions of fluid phases in the BB-model and the W-model. (a) aqueous phase production, (b)liquid organic phase production, (c) gaseous phase production.

6. Results of sensitivity and data-worth analyses

6.1. Effects of unknown reaction parameters

We performed a local sensitivity analysis to identify the most influential reaction parameters to the system responses. We selected the activation energies as the parameters to perturb in the sensitivity analysis, as they are most likely influential and at the same time highly uncertain (Bauman and Deo, 2010; Braun and Burnham, 1992).

After perturbing the activation energies of decomposition reactions, we observed the corresponding changes in system responses and the cumulative productions of hydrocarbons for both reaction models. The variation of the activation energy, used as the parameter scaling factor, was

set at 4.184 kJ mol^{-1} (= 1 kcal mol^{-1}). The standard deviations of the output observations, i.e., the uncertainties of the measurements, are listed in Table 4.

Table 4. Standard deviations of output observations: pressure [Pa], temperature [°C], scaled saturation of gaseous phase, scaled saturation of liquid organic phase, kerogen volume fraction, effective porosity, cumulative production of hydrocarbons [kg].

BB-model		**W-model**	
P	2.5E4	P	2.5E4
T	2.0	T	2.0
SO	0.01	SO	0.01
SG	0.01	SG	0.01
VKerogen	0.05	VKerogen	0.05
φeff	0.01	φeff	0.01
QHeavyoil	100	QHeavyoil	100
QLightoil	100	QLightoil	100
QC1gas	100	QC2gas	100
QC3gas	100		

Fig. 9 shows the scaled sensitivity coefficients of the system output at the monitoring point of $x = 2.52$ m and $y = 2.88$ m with respect to the activation energies of the decomposition reactions. Among the system responses, the scaled saturations of the liquid organic phase and the gaseous phase were the most sensitive to the activation energies of the decomposition reactions. The activation energy of the kerogen decomposition was the most influential parameter on the system responses. We observed the maximum absolute values of the scaled sensitivity coefficients between $t = 100$ and 200 days, when the reaction rate of kerogen decomposition peaked. As time advanced, the magnitudes of most scaled sensitivity coefficients did not continue to increase. Conversely, the sensitivity of the scaled saturation of gaseous phase to the activation energy of the heavy oil decomposition increased continuously until the end of the process. This was because heavy oil was still abundantly present until the end of the process, generating gases through the decomposition reaction.

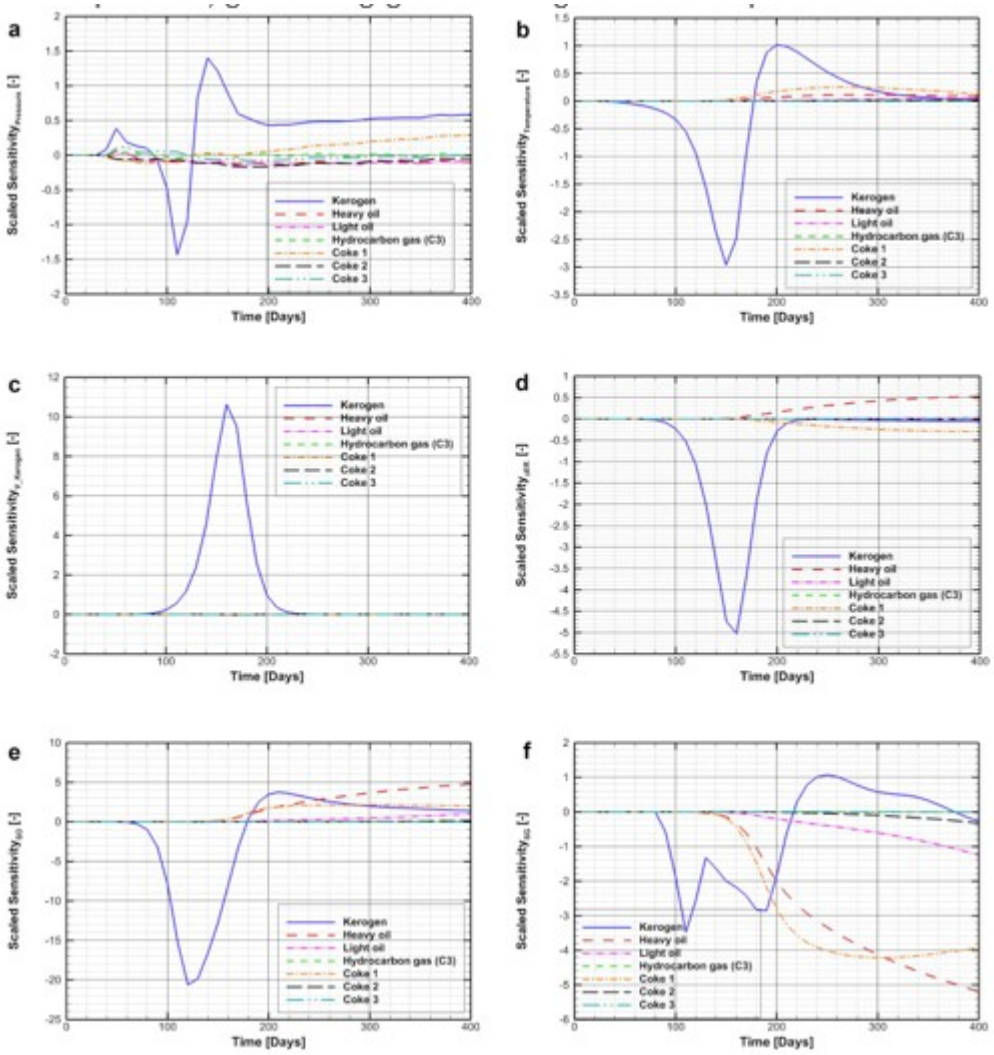

Fig. 9. BB-model: scaled sensitivity coefficients of system responses at the monitoring point, as a function of time with respect to the activation energies of decomposition reactions of kerogen, heavy oil, light oil, C3 gas, coke 1, coke 2, and coke 3. (a) pressure, (b) temperature, (c) kerogen volume fraction, (d) effective porosity, (e) scaled saturation of liquid organic phase, (f) scaled saturation of gaseous phase.

Table 5 presents the total scaled sensitivity coefficients of reactivity to the activation energies. Each reaction rate was most sensitive to the activation energy of its decomposition reaction. The activation energy of each reaction also significantly affected the reactivity of other reactions. This was because of the component interdependence, as the reactants of hydrocarbon and coke decompositions were the products in other reactions.

Table 5. Total scaled sensitivity coefficients of reactivity (reaction rate) to the activation energies of decomposition reactions for the BB-model. Note that the output scaling factors for the reaction rates of decomposition reactions were 1e-7, 1e-9, 1e-11, 1e-13, 1e-9, 1e-12, and 1e-15 $kg\,m^{-3}\,s^{-1}$.

	rKerogen	rHeavyoil	rLihtoil	rHCgas	rCoke1	rCoke2	rCoke3	**Total**
EKerogen	3.24e3	5.92e3	1.68e4	1.88e4	1.57e4	1.60e5	6.24e5	8.44

	rKerogen	rHeavyoil	rLihtoil	rHCgas	rCoke1	rCoke2	rCoke3	**Total**
								e5
EHeavyoil	2.77e0	1.63e4	1.67e4	3.19e4	1.09e3	1.79e5	6.14e5	8.59 e5
ELihtoil	3.11e-1	4.72e1	1.02e5	6.48e3	3.32e2	3.55e4	1.36e6	1.50 e6
EHCgas	4.06e-1	1.61e0	1.42e1	1.26e5	5.05e0	1.71e2	9.99e2	1.27 e5
ECoke1	7.10e0	9.41e2	1.22e4	5.69e3	5.84e4	2.02e6	7.22e6	9.32 e6
ECoke2	1.13e-1	3.30e1	4.48e2	1.20e3	1.10e2	3.13e6	1.14e7	1.45 e7
ECoke3	9.03e-2	9.77e-1	5.43e0	1.99e1	3.05e0	1.78e2	1.30e7	1.30 e7
Total	3.25e3	2.33e4	1.48e5	1.90e5	7.57e4	5.52e6	3.42e7	

Fig. 10 shows the sensitivity of the evolution of the hydrocarbon production to the activation energies of the decomposition reactions. Among the hydrocarbon components, the production of heavy oil was the most sensitive to the activation energies. In the sensitivity of C1 and C3 gas production, the effect of activation energy of coke 1 decomposition became the most significant at about $t = 200$ days. Unlike the other system responses in Fig. 9, the sensitivity of hydrocarbon production remained high or even increased as time advanced.

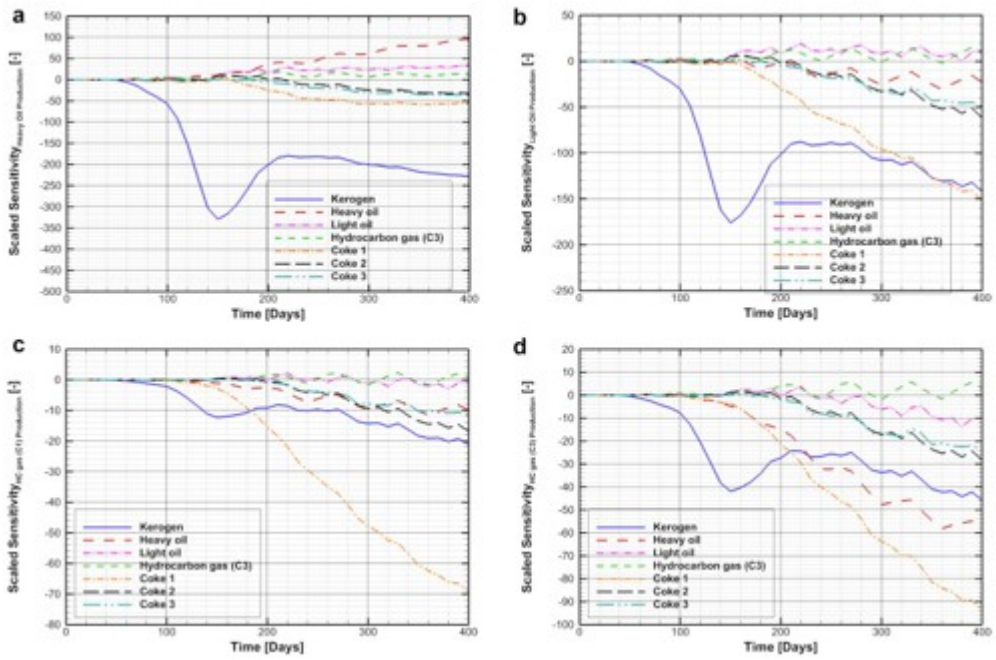

Fig. 10. BB-model: scaled sensitivity coefficients of cumulative production of hydrocarbon components with respect to the activation energies of decomposition reactions of kerogen, heavy oil, light oil, C3 gas, coke 1, coke 2, and coke 3. (a) heavy oil production, (b) light oil production, (c) C1 gas production, (d) C3 gas production.

Table 6 lists the total scaled sensitivity coefficients of the system responses, such as system states, dynamic properties, and hydrocarbon productions. From the total sensitivity, we select the most influential parameters and the most sensitive outputs. The six most significant parameters are the activation energies of kerogen, heavy oil, light oil, coke 1, coke 2, and coke 3 decompositions. The most sensitive outputs are the scaled saturations of liquid organic phase and gaseous phase, and cumulative production of every hydrocarbon component—heavy oil, light oil, C1 gas, and C3 gas. In the next section, we conduct a data-worth analysis using the selected influential parameters and sensitive outputs.

Table 6. Total sensitivity coefficients of system responses and hydrocarbon productions to the activation energies of decomposition reactions in the case of BB-model.

	P	T	Vkerogen	φeff	SO	SG	QHeavyoil	QLightoil	QC1gas	QC3gas	**Total**
EKerogen	2.05e1	2.09e1	4.68e1	2.44e1	1.59e2	3.63e1	6.58e3	3.52e3	3.82e2	1.00e3	1.18e4
EHeavyoil	3.52e0	2.24e0	3.04e-2	8.58e0	7.67e1	8.69e1	1.51e3	3.72e2	1.67e2	9.25e2	3.15e3
ELightoil	3.74e0	6.67e-1	3.42e-3	2.56e-1	1.12e1	1.40e1	6.52e2	2.79e2	2.54e1	1.25e2	1.11e3
EHCgas	5.54e-1	7.89e-3	5.31e-3	7.53e-3	1.04e-1	1.55e-1	3.11e2	1.89e2	2.59e1	6.76e1	5.94e2
ECoke1	4.78e0	4.76e0	1.13e-1	4.77e0	4.73e1	8.83e1	1.11e3	2.01e3	9.91e2	1.33e3	5.59e3
ECoke2	3.55e0	2.13e-1	1.57e-3	8.70e-2	1.23e0	2.61e0	4.69e2	6.51e2	1.80e2	3.21e2	1.63e3
ECoke3	1.49e0	3.51e-3	7.40e-4	1.92e-2	3.94e-2	4.18e-2	5.62e2	6.09e2	1.41e2	3.00e2	1.61e3
Total	3.82e1	2.87e1	4.69e1	3.82e1	2.96e2	2.28e2	1.12e4	7.64e3	1.91e3	4.07e3	

The sensitivity analysis results for the W-model are presented in Fig. 11, which shows the scaled sensitivity coefficients of the system responses to the activation energies of decomposition reactions. Similar to the results of the BB-model, the activation energy of kerogen decomposition was the most influential parameter, but the sensitivity to it was smaller than that of the BB-model. The most sensitive responses were the scaled saturations of the liquid organic phase and the gaseous phase.

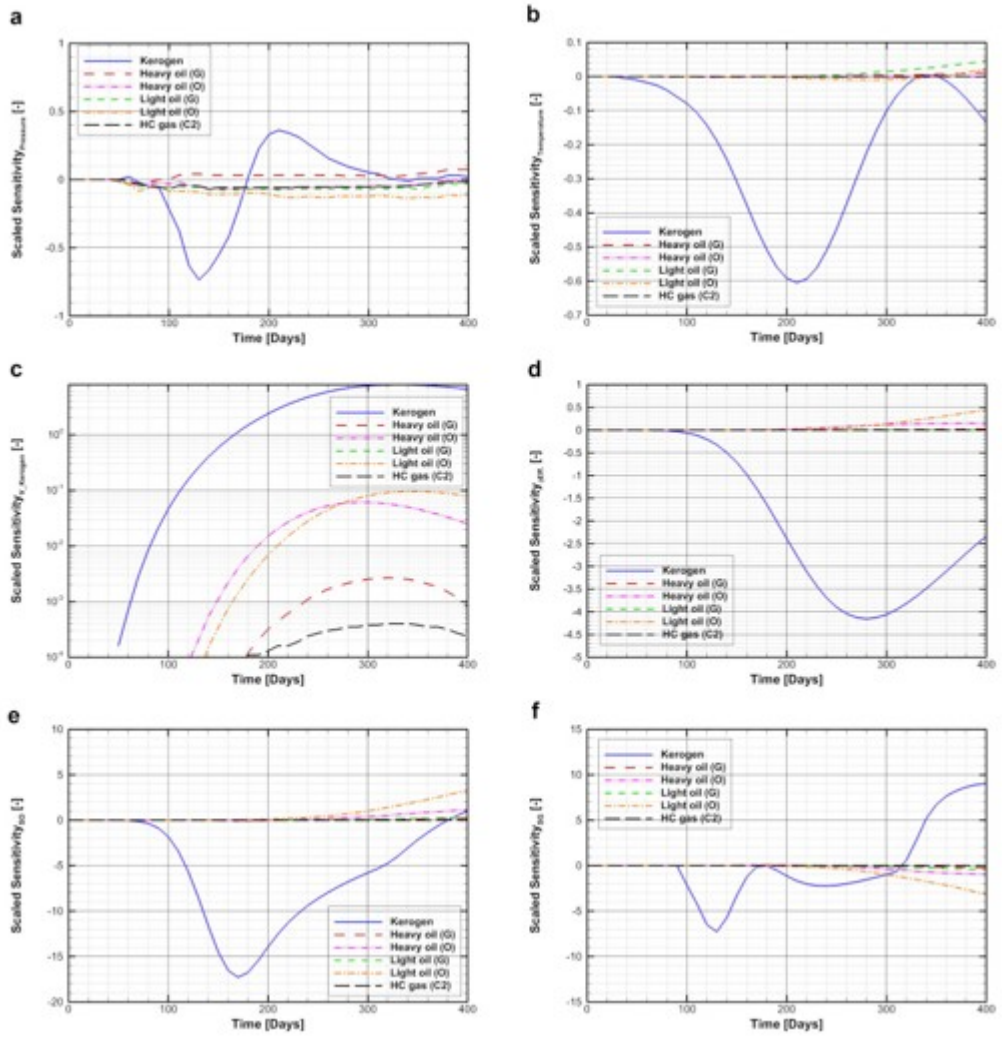

Fig. 11. W-model: scaled sensitivity coefficients of system responses at the monitoring point, as a function of time with respect to the activation energies of decomposition reactions of kerogen, heavy oil in gaseous phase, heavy oil in liquid organic phase, light oil in gaseous phase, light oil in liquid organic phase, and C2 gas. (a) pressure, (b) temperature, (c) kerogen volume fraction, (d) effective porosity, (e) scaled saturation of liquid organic phase, (f) scaled saturation of gaseous phase.

The total scaled sensitivities of reactivity of each decomposition reaction to the activation energies are shown in Table 7. Note that the reaction rate of heavy oil decomposition in the liquid organic phase was most sensitive to the activation energy of kerogen decomposition, rather than to its activation energy. The overall sensitivity coefficients of the W-model were lower than

those of the BB-model because the kerogen decomposition reaction, which generated the reactants of the subsequent “daughter” reactions, was more active in the BB-model.

Table 7. Total sensitivity coefficients of reactivity to the activation energies of decomposition reactions for W-model. Note that the output scaling factors for the reaction rates of decomposition reactions were 1e-7, 1e-9, 1e-8, 1e-9 1e-8, and 1e-13 $kg\,m^{-3}{\cdot}sec^{-1}$.

	rKerogen	rHeavyoil(G)	rHeavyoil(O)	rLightoil(G)	rLightoil(O)	rHCgas	**Total**
EKerogen	1.66e3	1.54e2	1.99e3	1.01e2	4.09e2	9.28e1	4.40e3
EHeavyoil(G)	2.77e-1	5.09e2	3.72e1	1.15e0	2.90e0	1.52e0	5.52e2
EHeavyoil(O)	3.35e-1	8.15e0	1.52e3	5.35e0	1.28e2	4.79e0	1.66e3
ELightoil(G)	1.25e0	2.39e0	3.68e0	3.31e2	7.64e0	3.75e0	3.49e2
ELightoil(O)	1.74e0	2.84e1	2.36e1	1.86e1	7.04e2	1.91e1	7.96e2
EHCgas	7.91e-2	2.92e-2	1.98e-1	1.98e-2	8.20e-2	2.48e2	2.48e2
Total	1.66e3	7.01e2	3.57e3	4.57e2	1.25e3	3.69e2	

Fig. 12 presents the scaled sensitivity coefficients of production of the various hydrocarbons to the activation energies. The cumulative production of light oil exhibited the most sensitive response among the productions of the various hydrocarbons. The activation energy of kerogen decomposition reaction was the most influential parameter throughout the heating and production period.

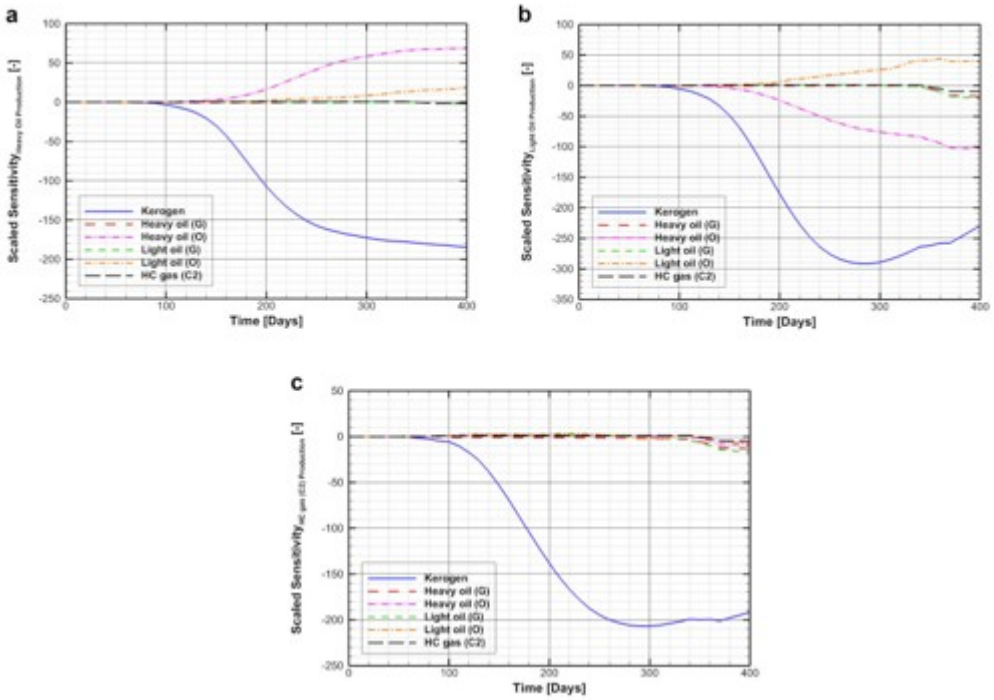

Fig. 12. W-model: scaled sensitivity coefficients of cumulative productions of hydrocarbon components with respect to the activation energies of decomposition reactions of kerogen, heavy oil in gaseous phase, heavy oil in liquid organic phase, light oil in gaseous phase, light oil in liquid organic phase, and C2 gas. (a) heavy oil production, (b) light oil production, (c) C2 gas production.

Table 8 lists the total scaled sensitivity coefficients of the system responses, such as system states, dynamic properties, and hydrocarbon productions. We select the activation energies of kerogen decomposition, heavy oil decomposition in liquid organic phase, and light oil decomposition in liquid organic and gaseous phases as the most influential parameters. The most sensitive outputs are the scaled saturations of liquid organic phase and gaseous phase, kerogen volume fraction, and cumulative production of every hydrocarbon component—heavy oil, light oil, and C2 gas. We conduct a data-worth analysis in the next section, using the selected influential parameters and sensitive outputs.

Table 8. Total sensitivity coefficients of system responses and hydrocarbon productions to the activation energies of decomposition reactions in the case of W-model.

	P	T	VKerogen	φeff	SO	SG	QHeavyoil	QLightoil	QC2gas	**Total**
EKerogen	6.69e0	8.03e0	1.40e2	7.95e1	2.36e2	1.08e2	3.80e3	6.00e3	4.58e3	1.50e4
EHeavyoil(G)	1.22e0	8.33e-2	3.59e-2	1.81e-1	1.79e0	1.95e0	1.33e1	9.22e1	9.96e1	2.10e2
EHeavyoil(O)	1.61e0	2.84e-2	9.34e-1	2.16e0	1.02e1	9.34e0	1.14e3	1.56e3	7.82e1	2.80e3
ELightoil(G)	2.11e0	3.69e-1	1.14e-1	2.28e-2	2.63e0	3.55e0	2.04e1	1.16e2	1.25e2	2.70e2
ELightoil(O)	3.82e0	1.72e-1	1.34e0	3.63e0	2.71e1	2.58e1	2.03e2	5.80e2	7.05e1	9.16e2
EHCgas	1.66e0	1.08e-2	6.77e-3	4.11e-3	1.73e-2	5.43e-2	1.29e1	6.10e1	4.96e1	1.25e2
Total	1.71e1	8.69e0	1.42e2	8.55e1	2.78e2	1.49e2	5.18e3	8.41e3	5.01e3	

6.2. Results of data-worth analysis

We performed a data-worth analysis to identify the most valuable data that need to be measured in order to reduce the uncertainty in the prediction of hydrocarbon production. Based on the sensitivity analysis, six unknown parameters were analyzed for both the BB- and the W-models. The corresponding observable variables (i.e., saturations, effective porosity, kerogen volume fraction, and cumulative productions) were obtained for a period of 300 days with data acquisition frequency of 10 days. The phase saturations, effective porosity, and kerogen volume fraction were obtained at the monitoring point of $x = 2.52\,\mathrm{m}$ and $y = 2.88\,\mathrm{m}$.

We predicted the total production of hydrocarbon components after the in-situ upgrading process at $t = 400$ days. The results of the data-worth analysis are presented in Table 9. The most valuable data to be measured for the most reliable prediction of total hydrocarbon production was the cumulative production of heavy oil in the BB-model and of the light oil in the W-model, respectively. This is consistent with the fact that these components show the highest contribution to overall production (Fig. 4, Fig. 6), and that they have the highest sensitivity to the unknown parameters (Fig. 10, Fig. 12) in each model. In both reaction models, measurement of the scaled saturations of the various phases and of the kerogen volume fraction did not significantly reduce the prediction uncertainty and thus these data were not considered valuable measurements to constrain the most influential parameters.

Table 9. Results of data-worth analysis. Note that the sum of all data worth is 100%.

Observation data	**Data worth ($\omega - k$) [%] for BB-model**	**Observation data**	**Data worth ($\omega - k$) [%] for W-model**
SO	0.05	SO	0.03
SG	0.16	SG	0.04
QHeavyoil	44.2	VKerogen	0.01
QLightoil	31.8	QHeavyoil	7.2
QC1gas	13.9	QLightoil	56.9
QC3gas	9.90	QC2gas	24.3

Table 10 shows the predictions of total hydrocarbon production. In both reaction models, total production of light oil was the most uncertain prediction. This was expected because light oil was generated from the most active reactions—kerogen and heavy oil decompositions. Comparing the two reaction models, the BB-model had lower prediction uncertainty, even though it produced a larger amount of hydrocarbons.

Table 10. Predictions of total hydrocarbon productions and prediction uncertainty.

Output predictions	Prediction at t = 400 days [kg] for BB-model	Standard deviation [kg] for BB-model	Output predictions	Prediction at t = 400 days [kg] for W-model	Standard deviation [kg] for W-model
QHeavyoil	1.36×10^5	70	QHeavyoil	2.42×10^4	84
QLightoil	1.13×10^5	108	QLightoil	9.55×10^4	294
QC1gas	1.87×10^4	51	QC2gas	6.30×10^4	236
QC3gas	4.39×10^4	49			

We conducted the data-worth analysis with respect to the observation times from 0 to 200, 250, 300, and 350 days. As previously, the phase saturations, effective porosity, and kerogen volume fraction were obtained at the monitoring point of $x = 2.52$ m and $y = 2.88$ m. The observation frequency was 10 days in each case. The results for the BB-model are shown in Fig. 13. In every case, the cumulative production of heavy oil showed the highest data worth, followed by the cumulative production of light oil. The relative data worth of the cumulative productions of hydrocarbon gases (C1 and C3) increased with increasing monitoring time. The scaled saturations of the liquid organic and of the gaseous phases showed insignificant data worth. Fig. 13 (b) shows the prediction uncertainties, as quantified by the standard deviations of total hydrocarbon productions at 400 days, with respect to the monitoring times. The total production of light oil had the highest prediction uncertainty in every case.

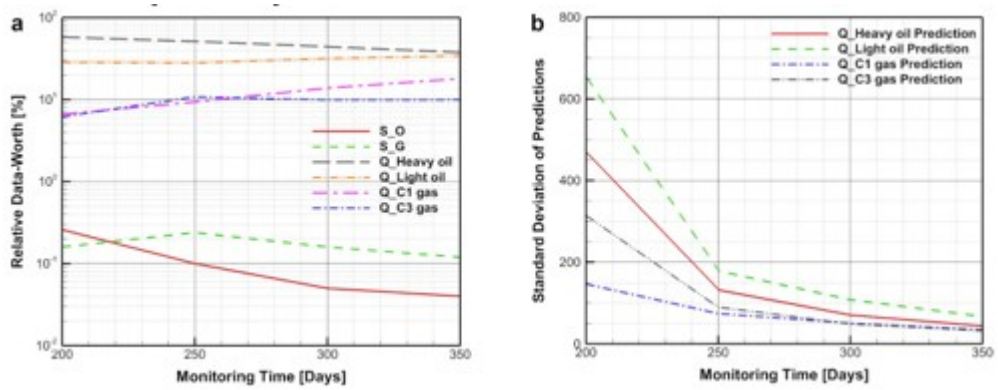

Fig. 13. Data worth as a function of monitoring time in the BB-model. (a) relative data worth of measurements, (b) uncertainty of predictions.

Data worth and prediction uncertainties for the W-model are provided in Fig. 14. For the short monitoring time of 200 days, observations of the kerogen volume fraction and of the scaled saturations of the liquid organic and of the gaseous phases showed higher data worth than the cumulative productions of hydrocarbons. With a longer monitoring time, measurement of hydrocarbon productions became important. For monitoring times longer

than 200 days, the cumulative production of light oil was the most valuable data for the prediction of total hydrocarbon production. Fig. 14 (b) shows the prediction uncertainty as a function of the monitoring time. To reduce prediction uncertainty significantly, we recommend the monitoring time to be at least 250 days. Once the maximum allowable uncertainty of prediction is determined, we can choose the most important observation data to be measured using Fig. 14 (a) and (b) as criteria.

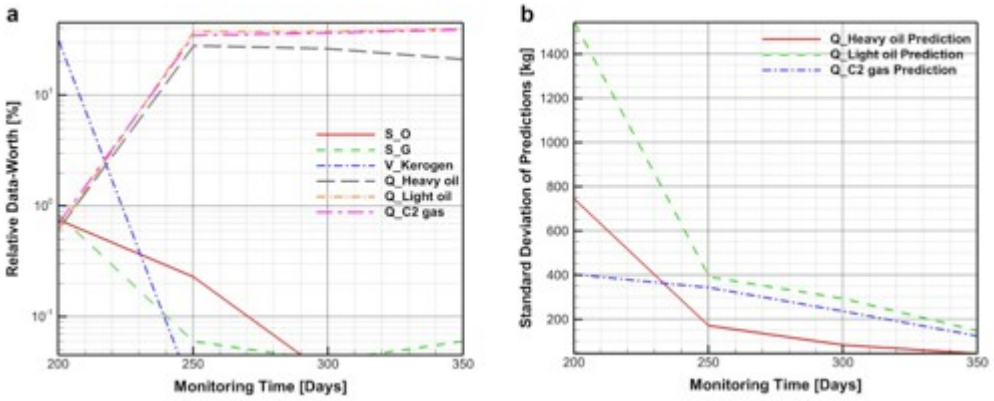

Fig. 14. Data worth as a function of monitoring time in the W-model. (a) relative data worth of measurements, (b) uncertainty of predictions.

The prediction of total hydrocarbon production was more uncertain when using the W-model, which required a longer monitoring time in order to obtain a prediction uncertainty similar to that of the BB-model. As can be seen in the earlier section on forward modeling, the slower start of hydrocarbon production in the W-model ($t = 100$ days) than in the BB-model ($t = 60$ days) caused the lower data worth of hydrocarbon productions for shorter monitoring times. This was because the data worth of each observation was affected by how sensitive the system response was to the unknown parameters; production data were not sensitive for a longer period in the W-model. Fig. 15 shows the prediction uncertainty of heavy oil and light oil in the BB-model and the W-model together. Both predictions were more uncertain in the W-model.

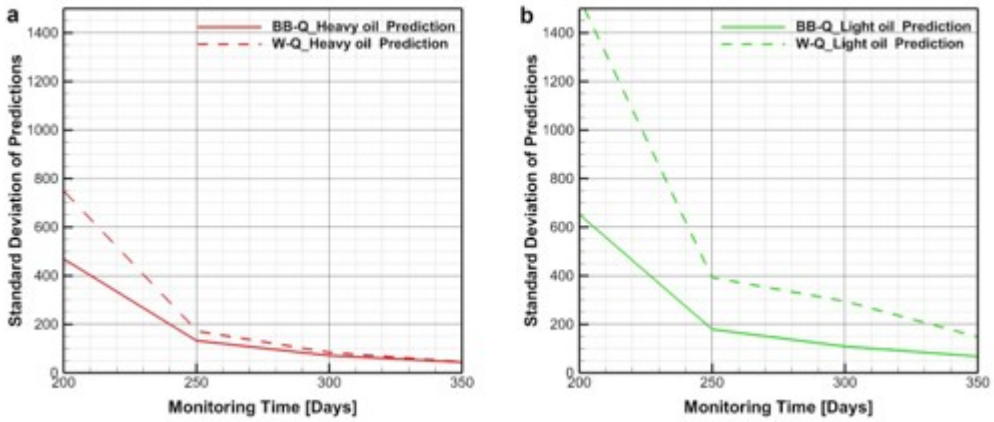

Fig. 15. Prediction uncertainty as a function of monitoring time in the BB-model and the W-model. (a) prediction of heavy oil production, (b) prediction of light oil production.

We repeated the data-worth analysis for different measurement uncertainties. The observation data were measured for 300 days with a measurement frequency of 10 days. In the case of the BB-model, we analyzed the effect of measurement uncertainty of the C1 gas production by using standard deviations of 50, 100, 150, and 200 kg.

Fig. 16 shows the results for the BB-model. The relative data worth of the cumulative productions of heavy oil, light oil, and C3 gas increased with an increasing uncertainty of measuring the C1 gas production. Note that the data worth of the scaled saturations of the liquid organic and gaseous phases had insignificant data worth (under 0.5%) and are not included in the plot. For an uncertainty in the C1 gas production of 150 and 200 kg, the data worth of C3 gas production was higher than that of C1. Fig. 16 (b) shows the prediction uncertainty of total hydrocarbon production as a function of measurement uncertainty of the C1 gas production. With increasing measurement uncertainty, the prediction uncertainty of the C1 gas production showed a large increase, but the prediction uncertainty of the production of the other hydrocarbons increased only slightly.

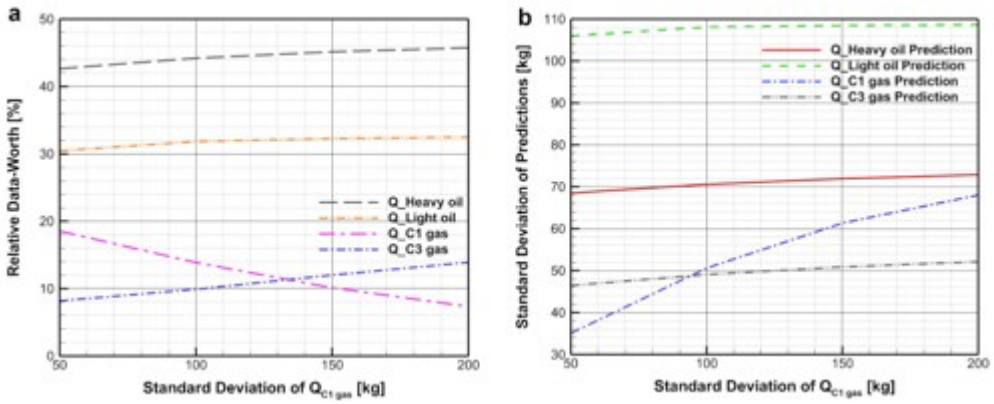

Fig. 16. Data worth as a function of measurement uncertainty in BB-model. (a) relative data worth of measurements, (b) uncertainty of predictions.

Similarly, we analyzed the effect of measurement uncertainty of the heavy oil productionwhen using the W-model and for standard deviations of 50, 100, 150, and 200 kg. Fig. 17 (a) shows that the data worth of the light oil and the hydrocarbon gas productions increased with an increasing measurement uncertainty of the heavy oil production. Note that the data worth of the kerogen volume fraction and of the scaled saturations of the liquid organic and the gaseous phases had insignificant data worth (under 0.05%) and, thus, were not included in the figure. Fig. 17 (b) shows the increasing prediction uncertainty of hydrocarbon productions. In every case, the most uncertain prediction was that of the light oil production. Once the expected measurement uncertainty is determined, we can select the data to be measured for the reduction of prediction uncertainty.

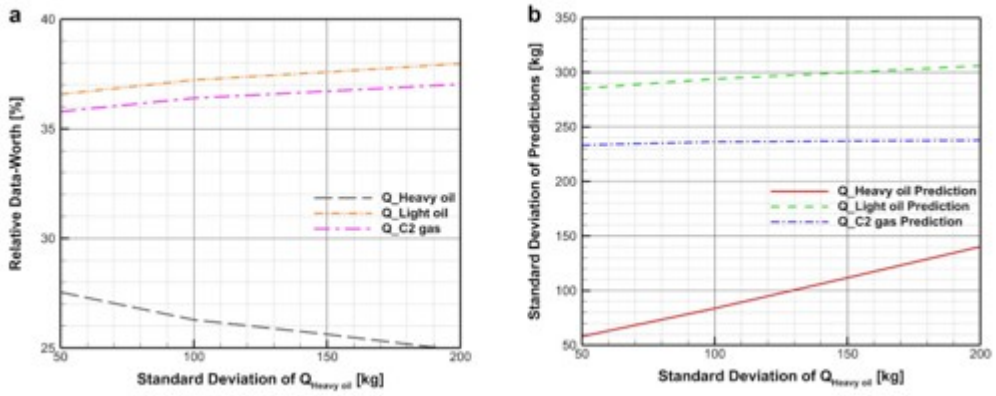

Fig. 17. Data worth as a function of measurement uncertainty in W-model. (a) relative data worth of measurements, (b) uncertainty of predictions.

7. Conclusions

In this study, we investigated the effects of the chemical reaction model and of the corresponding reaction parameters on the prediction uncertainty of hydrocarbon production from in-situ upgrading of oil shales. The issue was addressed by means of numerical simulation in combination with sensitivity and data-worth analyses.

The numerical simulation of heating and production processes were conducted by describing the Shell In-situ Conversion Process (ICP). From the simulation results, we quantitatively analyzed and compared the system responses and hydrocarbon productions using the BB-model and the W-model.

In addition to the numerical simulations, we quantified the effect of the generally unknown reaction parameters on the system responses and production behavior, and predicted the uncertainty of hydrocarbon production from measurable system responses. We conducted a local sensitivity analysis to identify the most influential reaction parameters and the most sensitive model output of interest. Using the selected set of reaction parameters and output behaviors, we conducted a data-worth analysis to identify the most valuable observations, i.e., the data that—if they were collected—significantly reduce the uncertainty of the prediction of hydrocarbon production.

The following conclusions can be drawn:

(1) The reaction of kerogen decomposition as well as subsequent decomposition reactions was more active in the BB-model. After 400 days of heating and production, the BB-model showed 1.3 times the amount of decomposed kerogen than the W-model.

(2) The BB-model resulted in a higher total hydrocarbon production than the W-model due to its more vigorous kerogen decomposition. Subsequent decomposition reactions were also more active in the BB-model, because of

their higher reaction rate constants and the resulting higher concentrations of reactants, which were generated from the kerogen decomposition.

(3) The results of the sensitivity analysis revealed that the most influential reaction parameters for the BB-model were the activation energies of the decomposition reactions of kerogen, coke 1, and heavy oil. The most sensitive system outputs were the cumulative productions of the various hydrocarbons.

(4) In the W-model, the most influential parameters were the activation energies of the decomposition reactions of kerogen, heavy oil in the liquid organic phase, and light oil in the liquid organic phase. The most sensitive system outputs were the cumulative productions of the various hydrocarbons.

(5) Comparing the two reaction models, we observe that the predictions of interest were sensitive to the activation energies of all reactions in the BB-model, while most of them were sensitive only to the activation energy of the kerogen decomposition in the W-model.

(6) The data-worth analysis provided the relative worth of observation data for the best prediction of total hydrocarbon production. Heavy oil production and light oil production were the most valuable data to predict the uncertainty of total hydrocarbon production when using either the BB-model or the W-model.

(7) Comparing the two reaction models, we determined that the prediction uncertainty obtained when using the BB-model was lower than that for the W-model. Once the allowable prediction uncertainty and expected measurement uncertainty are determined, we can select the appropriate observation data to be measured for the most reliable prediction of total hydrocarbon production. The reduction of the amount of measurement data can significantly reduce the monitoring cost.

(8) Envisioned studies will include the application of scaling analysis coupled with data-worth analysis for more general insights.

Acknowledgement

This study was conducted with the support of the Crisman Institute of the Petroleum Engineering Department at Texas A&M University. The authors also appreciate the funding sources of Lawrence Berkeley National Laboratory with the Office of Energy Efficiency and Renewable Energy and the Office of Fossil Energy of U.S. Department of Energy.

Nomenclature

Variables

U

internal energy

A_k
frequency factor
X
mass fraction
C
concentration of component
Δh_k
reaction enthalpy
Cp
specific heat capacity
μ
viscosity
Cpp
covariance matrix of estimated parameters
ρ
density
Czz
covariance matrix of output variables
σ_{pj}
parameter scaling factor
E_k
activation energy
σ_{zi}
output scaling factor
h
specific enthalpy
φ
media porosity
J
Jacobian matrix
$\omega - k$
relative data worth of observation

k
permeability
K
thermal conductivity
S
stoichiometric coefficient
Sβ
phase saturation
Sij
sensitivity coefficient
S¯ij
scaled sensitivity coefficient
T
temperature
Kk
reaction rate constant
M
mass change term
p
pressure
q
source/sink term
Q
cumulative production of hydrocarbon
rk
reaction rate
R
gas constant
Vectors
F
mass flux
g

gravity

Superscript

κ

component

Subscripts

A

aqueous phase

O

liquid organic phase

G

gaseous phase

S

solid phase

β

phase

References

Bauman and Deo, 2010

J.H. Bauman, M.D. Deo**Parameter space reduction and sensitivity analysis in complex thermal subsurface production processes**

Energy & Fuels, 25 (1) (2010), pp. 251-259

Braun and Burnham, 1990

R.L. Braun, A.K. Burnham**Mathematical model of oil generation, degradation, and expulsion**

Energy & Fuels, 4 (2) (1990), pp. 132-146

Braun and Burnham, 1992

R.L. Braun, A.K. Burnham**PMOD: a flexible model of oil and gas generation, cracking, and expulsion**

Org. Geochem., 19 (1–3) (1992), pp. 161-172

Burnham and Braun, 2017

A.K. Burnham, R.L. Braun**Simple relative sorptivity model of petroleum expulsion**

Energy & Fuels, 31 (9) (2017), pp. 9308-9318

Campbell et al., 1978

J.H. Campbell, G.H. Koskinas, N.D. Stout**Kinetics of oil generation from Colorado oil shale**

Fuel, 57 (6) (1978), pp. 372-376

Fan et al., 2010

Y. Fan, L. Durlofsky, H.A. Tchelepi**Numerical simulation of the in-situ upgrading of oil shale**

SPE J., 15 (02) (2010), pp. 368-381

Finsterle, 1999

S. Finsterle**iTOUGH2 User's Guide**

(1999)

LBNL-40040: 130

Finsterle, 2015

S. Finsterle**Practical notes on local data-worth analysis**

Water Resour. Res., 51 (12) (2015), pp. 9904-9924

Finsterle and Zhang, 2011

S. Finsterle, Y. Zhang**Solving iTOUGH2 simulation and optimization problems using the PEST protocol**

Environ. Model. Softw., 26 (7) (2011), pp. 959-968

Fowler and Vinegar, 2009

T.D. Fowler, H.J. Vinegar**Oil Shale ICP-Colorado Field Pilots, SPE Western Regional Meeting**

Society of Petroleum Engineers (2009)

Fucinos et al., 2017

R. Fucinos, D. Voskov, A.K. Burnham**Hierarchical Coarsening of Simulation Model for In-situ Upgrading Process, SPE Reservoir Simulation Conference**

Society of Petroleum Engineers (2017)

Krauss and Mays, 2014

E.D. Krauss, D.C. Mays**Modification of the Kozeny-carman equation to quantify formation damage by fines in clean, unconsolidated porous media**

SPE Reserv. Eval. Eng., 17 (04) (2014), pp. 466-472

Lee et al., 2018

K.J. Lee, S. Finsterle, G.J. Moridis**Estimating the reaction parameters of oil shale pyrolysis and oil shale grade using temperature transient analysis and inverse modeling**

J. Petroleum Sci. Eng. (2018)

Lee et al., 2016

K.J. Lee, G.J. Moridis, C.A. Ehlig-Economides**A comprehensive simulation model of kerogen pyrolysis for the in-situ upgrading of oil shales**

SPE J. (2016)

Lee et al., 2017

K.J. Lee, G.J. Moridis, C.A. Ehlig-Economides**Compositional simulation of hydrocarbon recovery from oil shale reservoirs with diverse initial saturations of fluid phases by various thermal processes**

Energy Explor. Exploitation, 35 (2) (2017), pp. 172-193

Maes et al., 2017

J. Maes, A.H. Muggeridge, M.D. Jackson, M. Quintard, A. Lapene**Scaling analysis of the In-Situ Upgrading of heavy oil and oil shale**

Fuel, 195 (2017), pp. 299-313

Moridis et al., 2006

G. Moridis, M. Kowalsky, S. Finsterle, K. Pruess**TOUGH+: the new generation of object-oriented family of codes for the soluation of problems of flow and transport in the subsurface**

Proceedings of the TOUGH Symposium (2006)

Ogunsola et al., 2010

O.I. Ogunsola, A.M. Hartstein, O. Ogunsola**Oil Shale: a Solution to the Liquid Fuel Dilemma. ACS Symposium Series, 1032**

American Chemical Society (2010)

325 pp

Parker et al., 1987

J. Parker, R. Lenhard, T. Kuppusamy**A parametric model for constitutive properties governing multiphase flow in porous media**

Water Resour. Res., 23 (4) (1987), pp. 618-624

Pepper and Corvi, 1995

A.S. Pepper, P.J. Corvi**Simple kinetic models of petroleum formation. Part I: oil and gas generation from kerogen**

Mar. Petroleum Geol., 12 (3) (1995), pp. 291-319

Pepper and Dodd, 1995

A.S. Pepper, T.A. Dodd**Simple kinetic models of petroleum formation. Part II: oil-gas cracking**

Mar. Petroleum Geol., 12 (3) (1995), pp. 321-340

Pruess, 1985

K. Pruess**A practical method for modeling fluid and heat flow in fractured porous media**

Soc. Petroleum Eng. J., 25 (01) (1985), pp. 14-26

Pruess et al., 1999

K. Pruess, C. Oldenburg, G. Moridis**TOUGH2 User's Guide Version 2**

Ernest Orlando Lawrence Berkeley National Laboratory, Berkeley, CA (US) (1999)

Reynolds et al., 1991

J.G. Reynolds, R.W. Crawford, A.K. Burnham**Analysis of oil shale and petroleum source rock pyrolysis by triple quadrupole mass spectrometry: comparisons of gas evolution at the heating rate of 10 C/min**

Energy fuels., 5 (3) (1991), pp. 507-523

Stone, 1970

H. Stone**Probability model for estimating three-phase relative permeability**

J. Petroleum Technol., 22 (02) (1970), pp. 214-218

Van Genuchten, 1980

M.T. Van Genuchten**A closed-form equation for predicting the hydraulic conductivity of unsaturated soils 1**

Soil Sci. Soc. Am. J., 44 (5) (1980), pp. 892-898

Vinegar, 2006

H. Vinegar**Shell's In-situ conversion process**

26th Oil Shale Symposium, Golden, Colorado, October 16 (2006), p. 2006

Wainwright and Finsterle, 2016

H.M. Wainwright, S. Finsterle**Global Sensitivity and Data-Worth Analyses in ITOUGH2**

Lawrence Berkeley National Laboratory (LBNL), Berkeley, CA (United States) (2016)

Wellington et al., 2005

S.L. Wellington, *et al.***In Situ thermal Processing of an Oil Shale Formation to Produce a Condensate**

(2005)

(Google Patents)

White et al., 2010

M. White, L. Chick, G. McVay**Impact of Geothermic Well Temperatures and Residence Time on the in Situ Production of Hydrocarbon Gases from green River Formation Oil Shale**

30th Oil Shale Symposium, Golden, CO, USA (2010)

Youtsos et al., 2013

M. Youtsos, E. Mastorakos, R. Cant**Numerical simulation of thermal and reaction fronts for oil shale upgrading**

Chem. Eng. Sci., 94 (2013), pp. 200-213